Tuijin Jishu/Journal of Propulsion Technology
ISSN: 1001-4055
Vol. 46 No. 2 (2025)

Potentials of Spaceborne Hyperspectral Data for Mineral Mapping: A Case Study of Rishabhdev, Rajasthan

Renu Chauhan[a*], Ronak Jain[a], Shiva Sharma[b]

[a]*School of Earth Sciences, Banasthali Vidyapith, Banasthali-304022, Rajasthan, India*

[b] *Csir-National Environmental Engineering Research Institute*

Abstract

The present study focuses on investigating the ultramafic suite of the Rishabhdev region using hyperspectral remote sensing techniques to identify potential sites for economic mineral exploration. Hyperspectral datasets will be employed to analyze the spectral characteristics of the rocks and associated minerals along the Rishabhdev lineament. This involves interpreting spectral signatures and conducting mineral mapping using tools such as band ratio imaging and other related methods. Preprocessing has been performed on the dataset and further standard methodology has been adopted for mineral mapping. Lizardite, kaolinite, and muscovite were identified as pure minerals and mapped in the region.

Keywords: *Ultramafic, Hyperspectral, Mineral.*

1. Introduction

The Rishabhdev Ultramafic Suite, located in southeastern Rajasthan between Serro-ki-pal and Sarkan (~55 km), lies at the contact between shelf and deep-sea facies of the Aravalli Supergroup. It is best exposed near Rishabhdev (24°10'N, 73°40'E) and Kherwara (24°05'N, 73°35'E). These rocks, striking NW–SE along a major lineament, are thought to represent obducted mantle peridotites or hydrothermally altered rocks, undergoing retrograde metamorphism. The suite is composed primarily of altered mafic–ultramafic rocks, including olivine (altered), serpentine, talc, carbonates (dolomite and magnesite), and iron oxides. The region is also mined for "green marble", talc, and soapstone. Geologically, these ultramafics are associated with meta sedimentary strata of the Aravalli Supergroup, consisting of quartzite, grit, and conglomerate, shale, dolomite, and limestone, interbedded with metamorphosed basaltic rocks (slate, phyllite, schist).To enhance mineral exploration, remote sensing techniques such as satellite imagery and aerial photography are employed. These methods, processed through software like ENVI and ERDAS, provide cost-effective, large-scale data acquisition, particularly in inaccessible areas. However, remote sensing results must be validated with field-based geological studies. Every material on Earth emits or reflects energy in the electromagnetic spectrum based on its unique spectral signature. For instance, hydrous vs. anhydrous minerals and Mg-rich vs. Fe-rich minerals exhibit different reflectance features, mainly in the 0.4–2.5 µm range. Atmospheric interference (e.g., at 1.4 µm due to water vapor) affects sensor readings. Multispectral sensors like Landsat and ASTER capture limited broad bands, while hyperspectral sensors like NASA's EO-1 Hyperion capture narrow, contiguous bands across the spectrum, offering higher spectral accuracy. Hyperspectral data is collected as a data cube, enabling detailed material discrimination. Although traditional geological methods (geochemistry, petrography, petrogenesis) have been applied to study this region, remote sensing applications remain limited. The current study aims to fill this gap

by exploring mineral compositions in the Rishabhdev ultramafic rocks using hyperspectral remote sensing techniques.

In this study, EO-1 Hyperion hyperspectral data was analyzed using the Spectral AngleMapper (SAM) algorithm to identify ultramafic minerals in the Rishabhdev region. The method was used to compare pixel spectra with reference spectra based on angular similarity, reducing the effect of illumination and enabling accurate mineral classification (Kruse et al., 1993).

2. Objectives

This study aims to closely examine the ultramafic rocks found in the Rishabhdev region using hyperspectral remote sensing technology. The goal is to identify different minerals, understand areas that have gone through changes like serpentinization, and locate zones that may contain valuable minerals. By combining satellite images with laboratory data, the study will create detailed mineral maps and highlight places that could be important for future mineral exploration and mining activities. This work will also help improve our understanding of the geology and structure of the area.

3. Study area

The area is located in between the latitude 24˚00’ to 25˚00’in the North and longitude 73˚00’ to 74˚00’ in the East in the geological map around Udaipur (Figure 1). The best exposures occur to the south-eastern Rajasthan around Rishabhdev (N 24º10': E 73º40') and Kherwara (N 24º05': E 73º35') (Purohit et al., 2015). The area is bounded by the Gujarat Border in the south and is surrounded by Aravalli range, which separates it from the Thar Desert.The area belongs to Palaeoproterozoic Aravalli Supergroup of rocks (Roy et al.,1988).Rocks around the study area produces great amount of green marbles, of which approximately 70% is being exported to different countries (Shekhawat, 2000). Undulating topography can be observed in the study area.

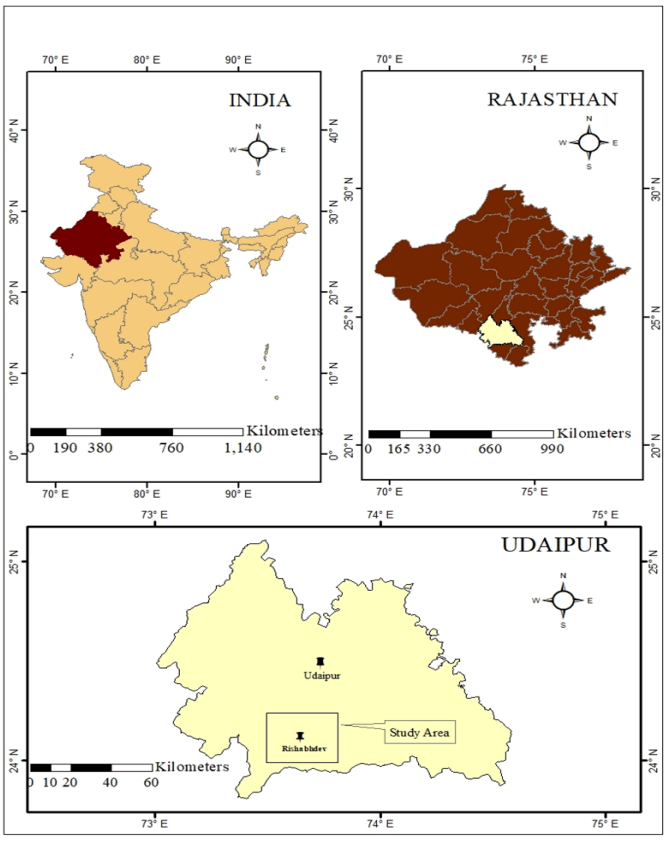

Figure1: Location Map of Study Area

Most of the area is covered by agricultural lands. Desert varnish can be noted on the outcrops of study area in the form of dark coatings (Kumar and Rajawat, 2020).Odwas,Parbeela,Kandula,Dewalkhas,Paldewal and area around Kherwara will be focused in the present study to fulfil the objective of the research (Figure 2).

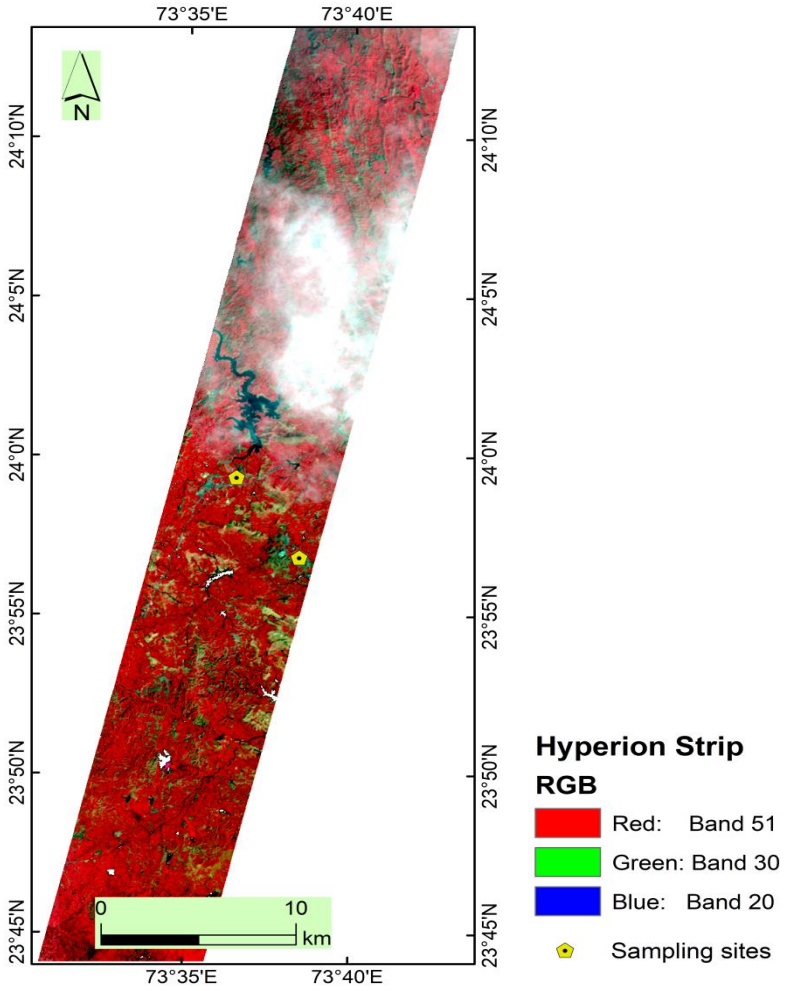

Figure2: False colour composite (FCC) image of Hyperion data strip obtained by assigning Red, Green and Blue colour to band 51, band 30 and band 20 bands. Yellow hexagonal is sampling sites

4. Literature review

Purohit et al. (2015) classified the Rishabhdev ultramafics into coarse-grained carbonate-talc-serpentine rocks, antigorite-chlorite rich rocks, and monomineralic chlorite forms. They noted compact, fine- to medium-grained greenish lithologies resembling altered carbonate rocks with dolomite, phyllite, and cherty quartzite. Olivine relicts and occurrences of magnetite, spinel, chromite, asbestos, and secondary sulphides were reported.Kumar and Rajawat (2020) used hyperspectral remote sensing and field studies to detect hydrothermally altered minerals like talc and dolomite. Spectral features (e.g., muscovite at 2.20 µm and lizardite) indicate low-temperature serpentinization (<350°C). Kaolinite and halloysite were found as alteration products of plagioclase in granite, while phyllites and quartzites showed muscovite and illite alteration.Mitra and Brahma (1988) conducted photogeologic mapping to identify structural and lithological features around Rishabhdev and Kherwara.

5. Materials and Methods

Hyperion, launched in 2000 aboard NASA's EO-1 satellite, was the first spaceborne hyperspectral sensor. Initially part of the New Millennium Program, its mission extended to 2017 due to research demand. It provides 242 spectral bands (0.357–2.576 µm) at 30 m resolution, using a push-broom imaging spectrometer. Data is freely available via USGS and NASA, with AIG and CSIRO supporting geological applications. The metadata for a Hyperion hyperspectral dataset acquired by the EO-1 (Earth Observing-1) satellite over the Rishabhdev region on October 2, 2012. The image, identified by the entity ID EO1H1480432012276110KZ_SGS_01, was captured during orbit path 149 and row 42, targeting path 148 and row 43. The scene acquisition began at 05:18:12 UTC and ended at 05:18:44 UTC, lasting approximately 32 seconds. The site is centered at latitude 24.34°N and longitude 73.72°E**,** corresponding to southern Rajasthan, India. The satellite operated at an inclination of 98.04°**,** which is typical of sun-synchronous orbits. Illumination conditions during the capture included a sun azimuth of 136.82° and a sun elevation of 53.50°, indicating favorable sunlight conditions for surface analysis. The image has a cloud cover of 20%**,** which may partially obscure the ground features. The data was processed to Level 1T (terrain-corrected)**,** ensuring both radiometric and geometric accuracy, making it suitable for direct application in geological and mineral mapping studies. The dataset is part of NASA's EO-1 mission and was made available through the USGS for research and analysis.

The flowchart presents a structured workflow for processing EO-1 Hyperion hyperspectral data aimed at mineral exploration through remote sensing (Figure 3). The process begins with the acquisition of EO-1 Hyperion data, which provides high-resolution spectral information across hundreds of narrow, contiguous bands. The next phase is pre-processing, which includes radiometric correction steps such as spatial and spectral subsetting to isolate the relevant portion of the image and de-striping to remove sensor-related noise artifacts. Following this, atmospheric correction is performed using the FLAASH (Fast Line-of-sight Atmospheric Analysis of Spectral Hypercubes) model to eliminate the effects of atmospheric gases and aerosols, ensuring accurate surface reflectance values.

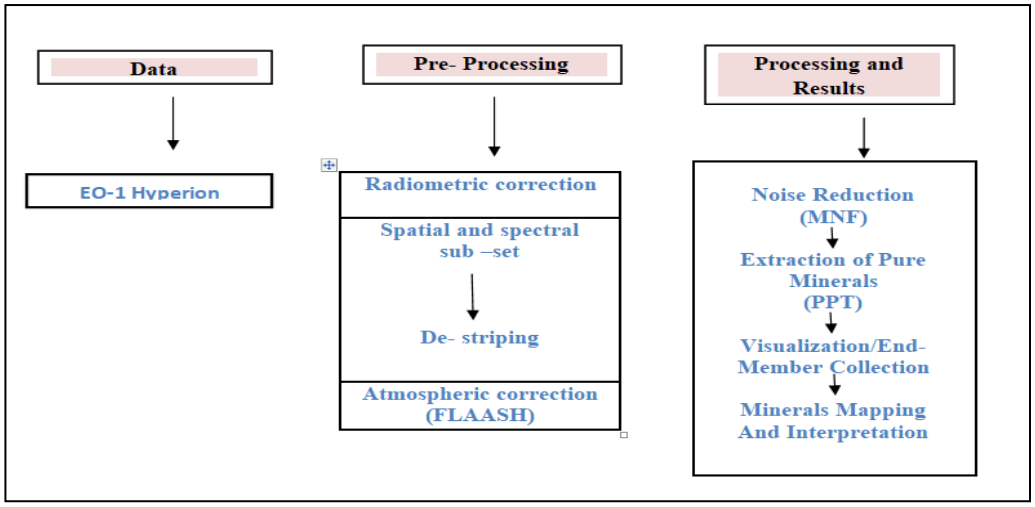

Figure 3: Flow Chart Showing Methodology.

Once the data is atmospherically corrected, it undergoes image enhancement techniques. These begin with noisereduction using the Minimum Noise Fraction (MNF) method, which helps isolate meaningful spectral information from noise. This is followed by the Pixel Purity Index (PPI) to detect spectrally pure pixels, which likely represent unique mineral signatures. These pure pixels are then visualized in n-dimensional (n-D) space forendmember collection**,** allowing the identification of distinct mineral types based on their spectral characteristics. The final step involves mineral mapping and interpretation, where the extracted spectral endmembers are used to generate thematic maps and infer the mineralogical composition of the region. This entire workflow enables detailed, non-invasive geological analysis, particularly beneficial in complex terrains such as the Rishabhdev ultramafic suite.

6. Results

6.1. Bad Band Removal

Hyperion dataset is consists of 242 bands. It has been examined that out of 242 bands some bands do not contain information. So, they must be discarded before proceeding for further processing techniques.In the table1, number of eliminated bands have been listed.

Table 1:List of Eliminated Bands.

Band Range	Reason for Elimination
1-7,209-242	Not Illuminated
58-76	Overlap Region
120-132,165-182,221-224	Water Vapour Absorption
98,116,134,164,188,189,191-196	Bands with noise

Some bands in the Hyperion dataset show bad columns due to sensor errors, resulting in zero or negative DN values. To correct this, the "Thor-destriping" tool in ENVI software is used, which replaces faulty pixel values with the average of neighboring pixels. Figure 4 illustrates this correction, with (a) showing the original image with bad columns and (b) showing the improved image after applying the de-striping filter.

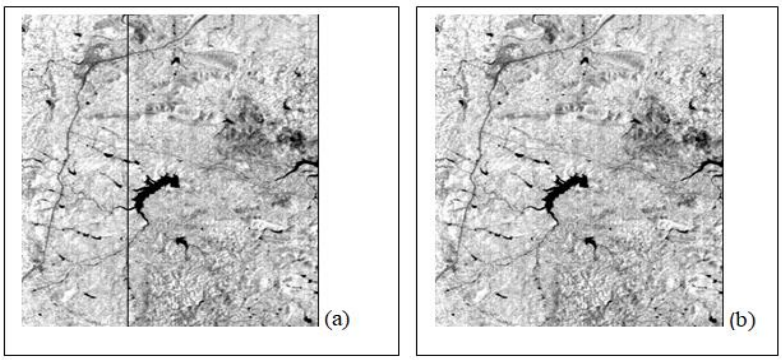

Figure 4: Data is showing bad column (a) and image data after bad column removal (b) for band 94.

6.2. Atmospheric Correction

Atmospheric correction was performed using ENVI's FLAASH module, which also converts radiance to reflectance. Required parameters are listed in Table 2. Figures 5 and 6 show noticeable changes in the image and pixel spectra after applying FLAASH.

Table2: Information Required for FLAASH Application

Attribute	**Value**
Site Lattitude	24°20'24"
Site Longitude	73°43'12"
Flight Date	2/10/ 2012
Flight Time	05:18:12
Sensor Altitude	705 km

Ground Elevation	0.7 km
Pixel Size	30 m
Atmospheric Model	Tropical
Aerosol Model	Rural

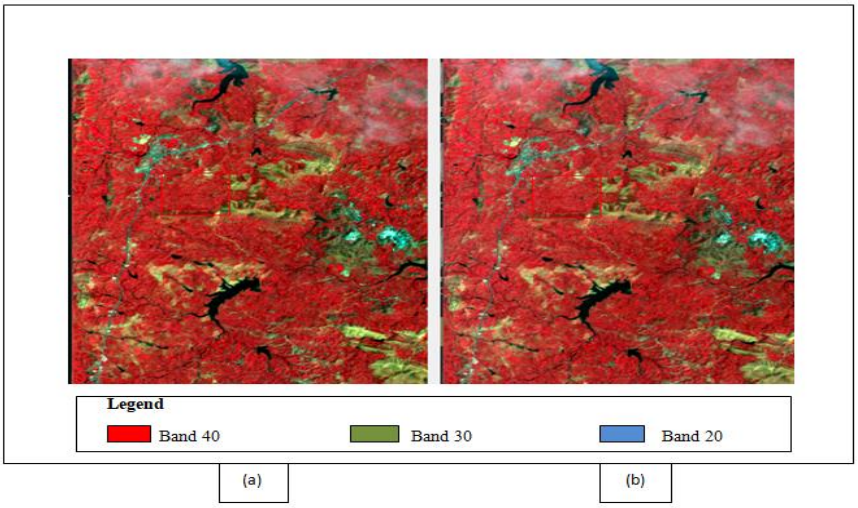

Figure 5: Image showing FCC image (a) after radiometric correction and FCC image (b) after applying FLAASH

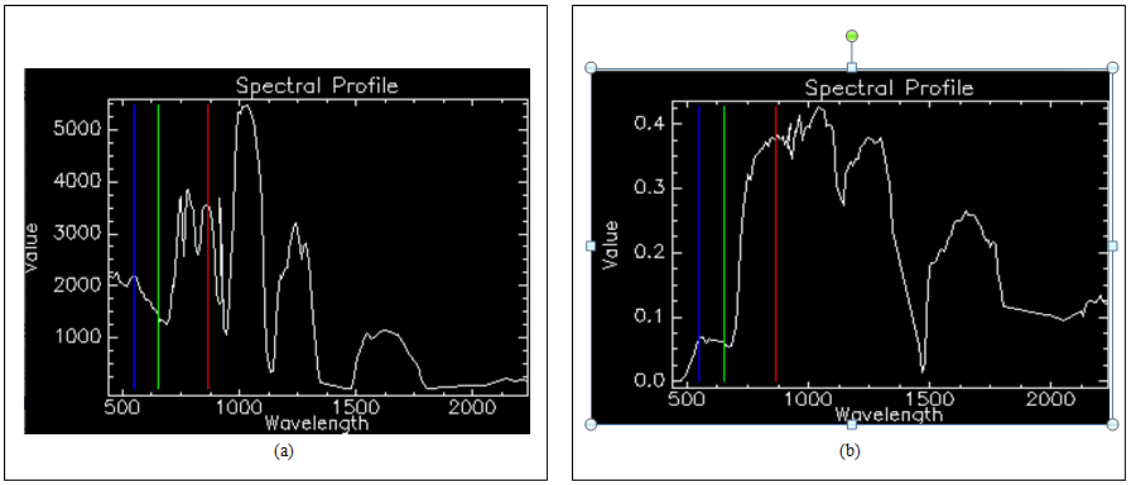

Figure 6: Vegetation spectra of a same pixel in the (a) radiometrically corrected image and (b) FLAASH corrected image, i.e., atmospherically corrected.

6.3. Minimum Noise Fraction

To reduce data noise, ENVI's Minimum Noise Fraction (MNF) tool was applied to the reflectance image from FLAASH. MNF separates noisy bands from informative ones and reduces data dimensionality. Figure 7 shows the eigenvalues plot, where only the first 10 bands with eigenvalues greater than one were selected for further processing. Figure 8 displays MNF images for bands 2, 3, 4, and 5, showing increasing noise from left to right as eigenvalues decrease.

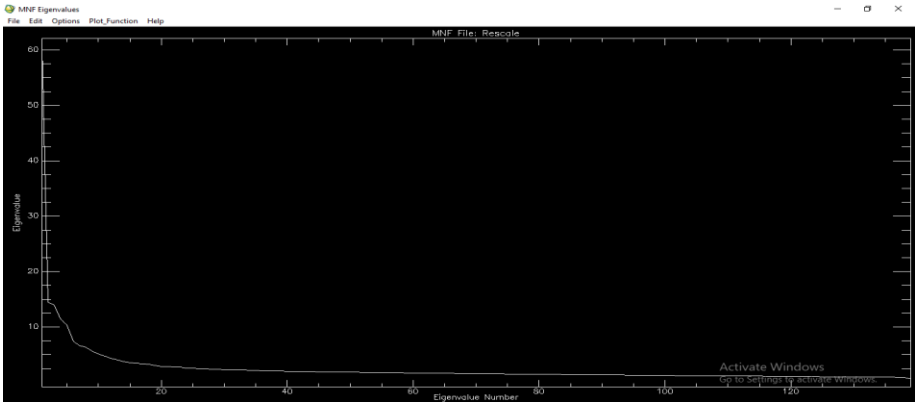

Figure 7: Eigen Value Plot for MNF Images

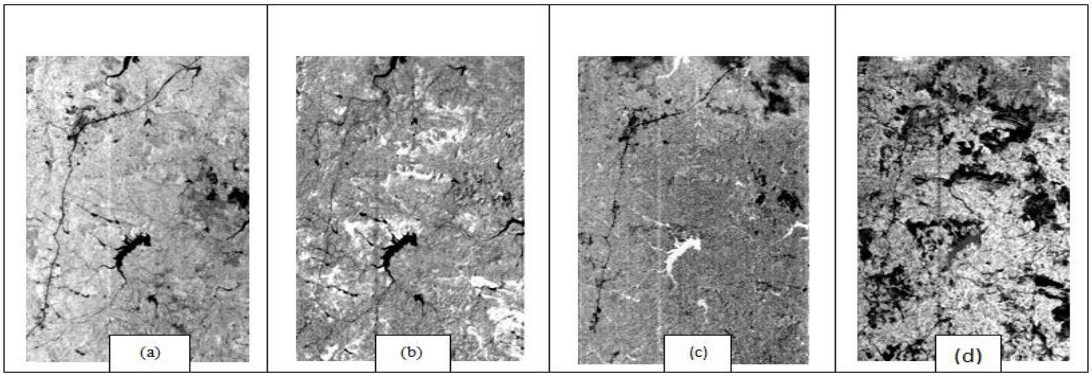

Figure8: MNF Images for bands (a) 2, (b) 3, (c) 4 and (d) 5

6.4. Pixel Purity Index

Pixel Purity Index (PPI) was applied to the first 10 MNF bands to identify extreme (pure) pixels, using 40,000 iterations and a threshold of 2.5. Figure 9shows the PPI result, where bright pixels indicate pure endmembers.

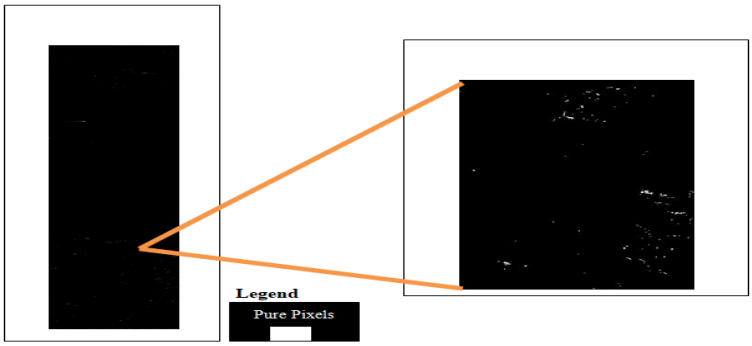

Figure 9: PPI image for Hyperion

6.5. n-Dimensional Visualization and End Member Collection

In the n-dimensional visualization process, pure pixel ROIs from the PPI image are loaded into the MNF result and rotated in multiple dimensions. Pixels appearing at the plot corners are marked as distinct end-member classes. Figure 10 shows the n-d scatter plot with colorful ROI points. The best spectra are selected as end-members based on their absorption-reflection features and comparison with the USGS spectral library.

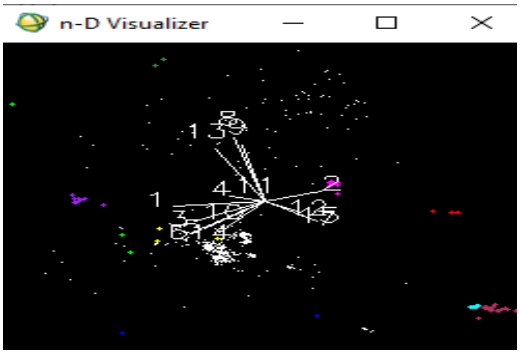

Figure 10: Plot for n-dimensional Visualization

6.6. End-member Collection

To map mineralogy, end-members lizardite, kaolinite, and muscovite were selected based on their unique absorption features (Figures 11 and 12). Kaolinite shows absorption near 1400, 2165, and 2200 nm due to OH and Al-OH, but lacks the 1900 nm water-related feature. Lizardite is identified by absorption near 1400–1500 nm and around 2150, 2200, and 2333 nm due to Mg-OH, helping distinguish it from chrysotile and antigorite. Muscovite shows key absorptions near 1400, 1900, 2200, and 2235 nm, related to metal-OH, water, and Al-OH bonds.

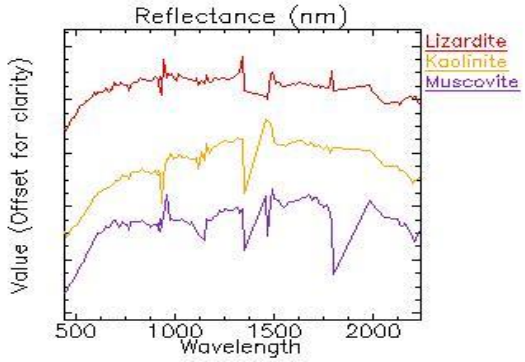

Figure 11: Spectral profile of end-members

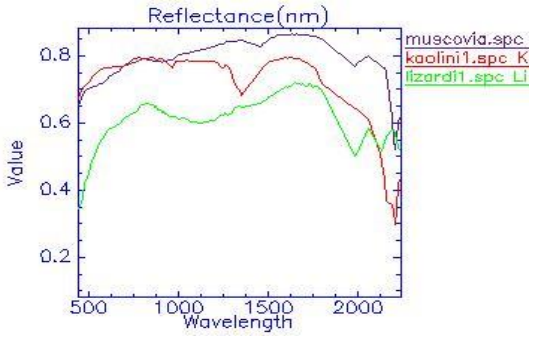

Figure 12: Spectral Plot USGS Library

6.7. Mineral Map

Hyperion hyperspectral data (357–2576 nm) enables precise mineral identification using absorption features (Figure 13). However, bands 2234–2576 nm was unusable due to sensor issues, affecting detection of some hydrous minerals like talc. Data quality was further reduced by spectral noise, mixed pixels, and desert varnish. Only one usable Hyperion strip was available, mostly showing altered zones. Despite limitations, end-members like lizardite, kaolinite, and muscovite were identified based on their spectral features.

Lizardite, a fine-grained phyllosilicate and member of the serpentine group ($Mg_3Si_2O_5(OH)_4$), typically forms from low-temperature hydrous alteration of mantle-derived Mg-silicates like peridotite. It appears green, with platy morphology, and often occurs with chrysotile and antigorite. Lizardite shows distinct spectral absorption near 1.4, 2.0, 2.15, 2.3, and 2.5 µm due to Mg–OH bonds, helping differentiate it from other serpentine minerals. In the current study, spectral angle mapping identifies lizardite near Kherwara and Paldewal.

Kaolinite, a dioctahedral clay mineral ($Al_2Si_2O_5(OH)_4$), forms through low-temperature alteration of feldspars in sedimentary rocks. It has a hardness of 2, dull earthy luster, and includes related minerals like nacrite and halloysite. Spectrally, kaolinite shows OH absorption near 1.4 µm and a doublet from Al–OH bonds at 2.16 and 2.20 µm, but lacks a 1.9 µm water peak due to low water content. Spectral mapping identifies kaolinite around Kherwara, Paldewal, Parbeela, and Dewalkhas as an alteration product of feldspar.

Muscovite, a mica group phyllosilicate ($KAl_2(AlSi_3O_{10})(OH)_2$), has perfect cleavage, 2–2.5 hardness, and vitreous luster. It forms through alteration in granites and pegmatites. Spectrally, it shows absorption near 1.4, 1.9, 2.20, and 2.35 µm due to OH, H_2O, and Al–OH bonds. Mapped mainly around Kherwara and Paldewal, muscovite, along with kaolinite and lizardite, indicates the area underwent low-grade metamorphism under water-rich, low-temperature, low-pressure conditions. Serpentine presence suggests alteration of mantle-derived ultramafics like dunite or peridotite, possibly from an ophiolite sequence (Kumar & Rajawat, 2020).

Figure 13: Mineral Map obtained from SAM. Lizardite: green colour; kaolinite: blue colour; muscovite: yellow colour.

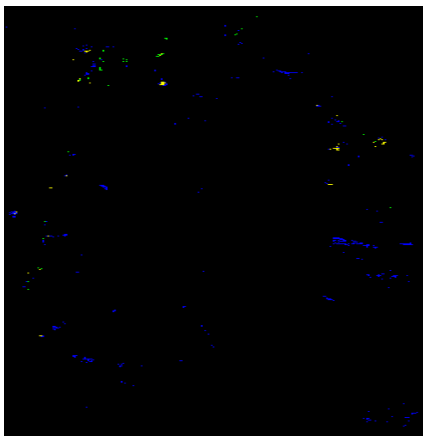

Conclusion

In this study, the Hyperion hyperspectral sensor was used to remotely investigate the Rishabhdev ultramafic suite. Using the Automated Identification of Group (AIG) technique, mineral alteration was mapped based on the detailed spectral information from Hyperion's narrow and continuous bands. However, some challenges were noted—such as desert varnish, dense vegetation, cloud cover, and overlapping spectral features—along with missing data in non-illuminated bands (e.g., 2234–2576 nm), which hindered detection of certain key alteration minerals like dolomite and talc. Despite these limitations, Hyperion proved effective in identifying end-members and assessing low-grade metamorphism and fluid interaction in the ultramafic rocks under water-saturated, low-temperature conditions.

References

1. Kumar, H., & Rajawat, A. S. (2020). Aqueous alteration mapping in Rishabdev ultramafic complex using imaging spectroscopy. International Journal of Applied Earth Observation and Geoinformation, 88, 102084.
2. Mitra, A., & Brahma, S. (1988). Photogeologic mapping north of Khairwara, Udaipur district, Rajasthan. Journal of the Indian Society of Remote Sensing, 16(2), 27-31.
3. Purohit, R., Bhu, H., Sarkar, A., & Ram, J. (2015). Evolution of the ultramafic rocks of the Rakhabdev and Jharol belts in southeastern Rajasthan, India: New evidences from imagery mapping, petro-minerological and OH stable isotope studies. Journal of the Geological Society of India, 85(3), 331-338.
4. Roy, A. B., & Jakhar, S. R. (2002). Geology of Rajasthan (Northwest India) precambrian to recent. Scientific Publishers.
5. Shekhawat, M. S. (2000). Derivatives of ultramafic rocks as decorative and dimensional stone in Rajasthan. Current Science, 78(7), 789-792.